STRUCTURAL BIOLOGY COMMUNICATIONS

ISSN 2053-230X

Crystal structure of cytoplasmic acetoacetyl-CoA thiolase from *Saccharomyces cerevisiae*

Pengfei Zhou, Zhongliang Zhu,* Muhammad Hidayatullah Khan, Peiyi Zheng, Maikun Teng and Liwen Niu*

Hefei National Laboratory for Physical Sciences at the Microscale and School of Life Sciences, University of Science and Technology of China, Hefei, Anhui 230026, People's Republic of China. *Correspondence e-mail: zlzhu63@ustc.edu.cn, lwniu@ustc.edu.cn

Received 7 October 2017
Accepted 25 November 2017

Edited by F. T. Tsai, Baylor College of Medicine, Houston, USA

Keywords: acetoacetyl-CoA thiolase; Claisen condensation; mevalonate pathway; X-ray crystallography; *Saccharomyces cerevisiae*.

PDB references: acetyl-CoA acetyltransferase, native, 5xz5; mutant, 5xyj

Supporting information: this article has supporting information at journals.iucr.org/f

Thiolases are vital enzymes which participate in both degradative and biosynthetic pathways. Biosynthetic thiolases catalyze carbon–carbon bond formation by a Claisen condensation reaction. The cytoplasmic acetoacetyl-CoA thiolase from *Saccharomyces cerevisiae*, ERG10, catalyses carbon–carbon bond formation in the mevalonate pathway. The structure of a *S. cerevisiae* biosynthetic thiolase has not previously been reported. Here, crystal structures of apo ERG10 and its Cys91Ala variant were solved at resolutions of 2.2 and 1.95 Å, respectively. The structure determined shows that ERG10 shares the characteristic thiolase superfamily fold, with a similar active-site architecture to those of type II thiolases and a similar binding pocket, apart from Ala159 at the entrance to the pantetheine-binding cavity, which appears to be a determinant of the poor binding ability of the substrate. Moreover, comparative binding-pocket analysis of molecule *B* in the asymmetric unit of the apo structure with that of the CoA-bound complex of human mitochondrial acetoacetyl-CoA thiolase indicates the canonical binding mode of CoA. Furthermore, the steric hindrance revealed in a structural comparison of molecule *A* with the CoA-bound form raise the possibility of conformational changes that are associated with substrate binding.

1. Introduction

Thiolases are vital ubiquitous enzymes which catalyze the formation of carbon–carbon bonds *via* a Claisen condensation reaction. Thiolases catalyze the acetylation of a reactive cysteine residue followed by a condensation reaction, which is the major enzymatic route of fatty-acid, polyketide and steroid synthesis (Haapalainen *et al.*, 2006). Thiolases have been divided into degradative thiolases (EC 2.3.1.16) and synthetic thiolases (EC 2.3.1.9) based on their biological functions and substrate specificity (Modis & Wierenga, 1999). Degradative thiolases, which are also termed 3-ketoacyl-CoA thiolases, exhibit broad chain substrate specificity, while biosynthetic thiolases or acetoacetyl-CoA thiolases are highly specific for short-chain substrates such as acetyl-CoA and acetoacetyl-CoA (Kursula *et al.*, 2005).

The *Saccharomyces cerevisiae* degradative peroxisomal thiolase is involved in fatty-acid β-oxidation and the implications of its structure for substrate binding and reaction mechanism have been reported (Mathieu *et al.*, 1997). In contrast, the cytoplasmic acetoacetyl-CoA thiolase from *S. cerevisiae* (ERG10) catalyses the first step of the mevalonate pathway by a reversible nondecarboxylative condensation reaction in which acetoacetyl-CoA is synthesized from two molecules of acetyl-CoA (Jiang *et al.*, 2008). All isoprene-containing compounds such as sterols, quinones,

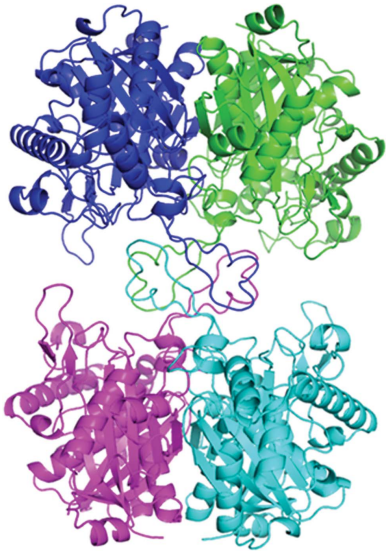

Table 1
Macromolecule-production information.

Protein	ERG10	Cys91Ala mutant
Source organism	*S. cerevisiae* (strain ATCC 204508/S288c)	*S. cerevisiae* (strain ATCC 204508/S288c)
DNA source	Genomic DNA	Plasmid ERG10 in pET-22bN
Forward primer†	5′-TTCCATATGTCTCAGAACGTTTAC-3′	5′-AAGGTCTCTGCATCCGCTATGAAGGCAATC-3′
Reverse primer‡	5′-CCGCTCGAGTCATATCTTTTCAATGACAATAG-3′	5′-TAGCGGATGCAGAGACCTTGTTAACTGTGC-3′
Cloning vector	pET-22bN	pET-22bN
Expression vector	pET-22bN	pET-22bN
Expression host	*E. coli* BL21 (DE3)	*E. coli* BL21 (DE3)
Complete amino-acid sequence of the construct produced§	MG*HHHHHH*GSHMSQNVYIVSTARTPIGSFQGSLSSKTAVE GSHMSQNVYIVSTARTPIGSFQGSLSSKTAVELGAVAL KGALAKVPELDASKDFDEIIFGNVLSANLGQAPARQVA LAAGLSNHIVASTVNKVCASAMKAIILGAQSIKCGNAD VVVAGGCESMTNAPYYMPAARAGAKFGQTVLVDGVERD GLNDAYDGLAMGVHAEKCARDWDITREQQDNFAIESYQ KSQKSQKEGKFDNEIVPVTIKGFRGKPDTQVTKDEEPA RLHVEKLRSARTVFQKENGTVTAANASPINDGAAAVIL VSEKVLKEKNLKPLAIIKGWGEAAHQPADFTWAPSLAV PKALKHAGIEDINSVDYFEFNEAFSVVGLVNTKILKLD PSKVNVYGGAVALGHPLGCSGARVVVTLLSILQQEGGK IGVAAICNGGGGASSIVIEKI	MG*HHHHHH*GSHMSQNVYIVSTARTPIGSFQGSLSSKTAVE GSHMSQNVYIVSTARTPIGSFQGSLSSKTAVELGAVAL KGALAKVPELDASKDFDEIIFGNVLSANLGQAPARQVA LAAGLSNHIVASTVNKV**A**ASAMKAIILGAQSIKCGNAD ASAMKAIILGAQSIKCGNADVVVAGGCESMTNAPYYMP AARAGAKFGQTVLVDGVERDGLNDAYDGLAMGVHAEKC ARDWDITREQQDNFAIESYQKSQKSQKEGKFDNEIVPV TIKGFRGKPDTQVTKDEEPARLHVEKLRSARTVFQKEN GTVTAANASPINDGAAAVILVSEKVLKEKNLKPLAIIK GWGEAAHQPADFTWAPSLAVPKALKHAGIEDINSVDYF EFNEAFSVVGLVNTKILKLDPSKVNVYGGAVALGHPLG CSGARVVVTLLSILQQEGGKIGVAAICNGGGGASSIVI EKI

† The NdeI site is underlined. ‡ The XhoI site is underlined. § The His_6 tag is in shown in italics. The amino acid in bold indicates the position of the mutation.

dolichol and isopentenylated adenosine in tRNAs are products of this pathway. Ergosterol was found to be the major sterol product of this pathway (Hiser *et al.*, 1994).

Various structures of human and bacterial thiolases in complexes with their substrates have been resolved to investigate the binding mode of the substrates and their catalytic mechanisms, but the structure of a synthetic thiolase from a lower eukaryote such as *S. cerevisiae* as yet remains unexplored. After we had resolved the crystal structure of the wild-type thiolase, we attempted to obtain the complex of the Cys91Ala mutant thiolase with CoA by co-crystallization, but no obvious density for CoA was observed. The current work concludes that ERG10 shares a similar overall structure with biosynthetic thiolases and also possesses a conserved Cys–Asn–His catalytic triad in addition to another Cys residue that acts as a base. Comparative analysis of the binding pockets between molecule *B* of the asymmetric unit and human mitochondrial acetoacetyl-CoA thiolase (T2) reveals a highly typical interaction behaviour for ERG10 and CoA, with the exception of Ala159. The clashes that result on docking CoA into molecule *A* of the asymmetric unit reveal conformational changes on CoA binding.

2. Materials and methods

2.1. Recombinant protein production

The gene encoding native ERG10 was amplified by PCR from *S. cerevisiae* genomic DNA and cloned into pET-22bN vector using NdeI and XhoI sites to encode recombinant protein with a hexahistidine tag at the N-terminus. The Cys91Ala mutant was obtained by site-directed mutagenesis utilizing the resulting plasmid as a template, as reported by Sato *et al.* (1998). Both recombinant plasmids were transformed into *Escherichia coli* BL21 (DE3) cells for expression. Protein expression was induced at 289 K for approximately 20 h by adding 0.5 m*M* isopropyl *β*-D-1-thiogalactopyranoside (IPTG). Bacterial cells were harvested by centrifugation at 6080*g* for 6 min, resuspended in buffer *A* (50 m*M* Tris–HCl pH 8.0, 500 m*M* NaCl, 5% glycerol) and disrupted by sonication *via* an ultrasonicator (Qsonica, USA). Cell debris was removed by ultracentrifugation (20 000*g* for 30 min at 277 K) and the recombinant protein was purified from the supernatant using a two-step purification protocol consisting of Ni^{2+}-affinity chromatography (Ni^{2+}–NTA column; GE Healthcare, USA) and size-exclusion chromatography (HiLoad 16/60 Superdex 200 column; GE Healthcare, USA). The same procedure was used to purify the Cys91Ala mutant. Prior to crystallization, both protein samples were diluted to 10 mg ml^{-1} in buffer *B* (20 m*M* Tris–HCl pH 8.0, 200 m*M* NaCl, 5% glycerol). The mutant protein was incubated at room temperature with CoA at a molar ratio of 1:10 for 1 h. Macromolecule-production information is summarized in Table 1.

2.2. Crystallization

The hanging-drop vapour-diffusion method was used for initial crystallization screening utilizing various conditions. Both the native and the mutant protein crystallized in several conditions. The drops were prepared using 1.0 µl protein sample and an equal volume of crystallization reservoir solution and were equilibrated against 100 µl precipitant solution as described in Table 2.

2.3. X-ray data collection and processing

The crystal was fished out with a clean loop and flash-cooled in liquid nitrogen at 100 K using reservoir solution containing 20%(*v*/*v*) glycerol as a cryoprotectant. X-ray diffraction data sets for the wild-type and mutant thiolases were collected on beamlines BL17U1 and BL18U1 at Shanghai Synchrotron

Table 2
Crystallization.

Protein	ERG10	Cys91Ala mutant
Method	Hanging-drop vapour diffusion	Hanging-drop vapour diffusion
Plate type	24-well plate (Hampton Research)	24-well plate (Hampton Research)
Temperature (K)	287	287
Protein concentration (mg ml^{-1})	10	10
Buffer composition of protein solution	20 m*M* Tris–HCl pH 8.0, 200 m*M* NaCl, 5% glycerol	20 m*M* Tris–HCl pH 8.0, 200 m*M* NaCl, 5% glycerol
Composition of reservoir solution	0.2 *M* ammonium citrate pH 7.0, 17% PEG 3350	0.2 *M* ammonium citrate pH 6.5, 19% PEG 3350

Table 3
Data collection and processing.

Values in parentheses are for the highest resolution shell.

Protein	ERG10	Cys91Ala mutant
Diffraction source	BL17U1, SSRF	BL18U1, SSRF
Wavelength (Å)	0.97916	0.97778
Temperature (K)	100	100
Detector	ADSC Q315R	PILATUS 6M
Crystal-to-detector distance (mm)	300	300
Rotation range per image (°)	1	1
Total rotation range (°)	360	360
Exposure time per image (s)	1	0.3
Space group	$P2_12_12$	$P2_12_12$
a, *b*, *c* (Å)	77.25, 88.65, 123.42	78.80, 89.25, 119.19
α, β, γ (°)	90, 90, 90	90, 90, 90
Resolution range (Å)	50.0–2.20 (2.24–2.20)	50.0–1.95 (1.98–1.95)
No. of unique reflections	43320 (2111)	62459 (3038)
Completeness (%)	99.7 (100.0)	98.8 (98.1)
Multiplicity	8.3 (8.0)	8.8 (8.3)
$\langle I/\sigma(I)\rangle$	19.4 (4.2)	18.7 (5.1)
$R_{\rm merge}$†	0.09 (0.52)	0.10 (0.52)
Overall *B* factor from Wilson plot (Å^2)	33.3	15.6

† $R_{\rm merge} = \sum_{hkl}\sum_i |I_i(hkl) - \langle I(hkl)\rangle| / \sum_{hkl}\sum_i I_i(hkl)$, where $I_i(hkl)$ is the intensity of reflection *hkl* and $\langle I(hkl)\rangle$ is the average value for reflection *hkl*.

Radiation Facility (SSRF). The available data sets were indexed, integrated and scaled using the *HKL*-2000 program suite (Otwinowski & Minor, 1997). Data-collection and processing statistics are detailed in Table 3.

2.4. Structure solution and refinement

MOLREP from the *CCP*4 program suite (Vagin & Teplyakov, 2010) was used to solve the structure of ERG10 by the molecular-replacement method using a single monomer of the tetrameric human mitochondrial thiolase (PDB entry 2ib7; Haapalainen *et al.*, 2007) as a search model. The final structure model was completed by alternating manual building in *Coot* (Emsley *et al.*, 2010) and restrained refinement in *REFMAC*5 (Murshudov *et al.*, 2011). An overall assessment of the model quality was made using the structure-validation program *PROCHECK* (Laskowski *et al.*, 1993). The same procedure was also applied to resolve the structure of the Cys91Ala mutant. The refinement and stereochemical statistics for the two structures are summarized in Table 4. The atomic coordinates and structure factors were deposited in the PDB as entries 5xz5 and 5xyj for the wild-type and mutant thiolases, respectively. Figures showing structures were prepared using *PyMOL* (DeLano, 2002).

Table 4
Structure solution and refinement.

Protein	ERG10	Cys91Ala mutant
Resolution range (Å)	50.0–2.20 (2.24–2.20)	50.0–1.95 (1.98–1.95)
Completeness (%)	99.7 (100.0)	98.8 (98.1)
$R_{\rm work}$†	0.1869	0.1557
$R_{\rm free}$‡	0.2242	0.1718
R.m.s.d.§		
Bonds (Å)	0.007	0.006
Angles (°)	1.266	1.252
Average *B* factor (Å^2)	43.5	22.7
No. of water molecules	364	809
Ramachandran plot¶		
Most favoured region (%)	92.5	93.5
Additionally allowed region (%)	6.75	5.7
Generously allowed region (%)	0.45	0.3
Disallowed region (%)	0.3	0.3

† $R_{\rm work} = \sum_{hkl} ||F_{\rm obs}| - |F_{\rm calc}|| / \sum_{hkl} |F_{\rm obs}|$, where $F_{\rm obs}$ and $F_{\rm calc}$ are the observed and calculated structure-factor amplitudes, respectively. ‡ $R_{\rm free}$ is the same as $R_{\rm work}$ but for a 5% subset of all reflections that were not used in crystallographic refinement. § Root-mean-square deviation from ideal values. ¶ The categories were defined by *PROCHECK*.

3. Results and discussion

3.1. Oligomerization

The apparent molecular weight of wild-type ERG10 in solution was determined by comparison with protein standards of precisely known molecular weights using a HiLoad 16/60 Superdex 200 column. The elution volumes of protein standards were used to calculate a standard curve. The elution volume (63.07 ml) of the predominant peak corresponds to an apparent molecular weight of 164 kDa for ERG10, which coincides with the result reported by Kornblatt & Rudney (1971) and demonstrates the tetrameric state of ERG10 in solution (Fig. 1).

3.2. Overall structure and active site

The asymmetric unit of the crystal contains two protomers, but a tetramer similar to those found in type II biosynthetic thiolases such as mitochondrial thiolase (T2) from *Homo sapiens* (Haapalainen *et al.*, 2007) and cytoplastic thiolase (bCT) from *Zoogloea ramigera* (Modis & Wierenga, 2000) could be constructed by applying crystallographic symmetry operations (Fig. 2*a*) and is shown not to be a crystallographic artefact by the tetrameric state in solution. In essence, the structure of ERG10 is similar to those of T2 and bCT, even to the level of details of the quaternary-structure organization. Each subunit of ERG10 consists of N-terminal, C-terminal and loop domains. The active site is constructed on the

N-terminal and C-terminal domains and its identical architecture to those of T2 and bCT reveals that the catalytic mechanism of ERG10 is similar to those of type II thiolases. The loop domain plays multiple roles in shaping the binding pocket for the CoA moiety of the substrate, stabilizing the tetramer and covering the active-site cavity using a tetramerization loop and a covering loop, respectively (Fig. 2*b*). Although the overall structure of ERG10 is highly similar to those of T2 and bCT, it differs in the following three key aspects: (i) the presence of Ala159 at the entrance to the pantetheine-binding cavity, (ii) the presence of a disordered region in molecule *A* of the asymmetric unit and (iii) the steric clashes that are observed on docking CoA into molecule *A*.

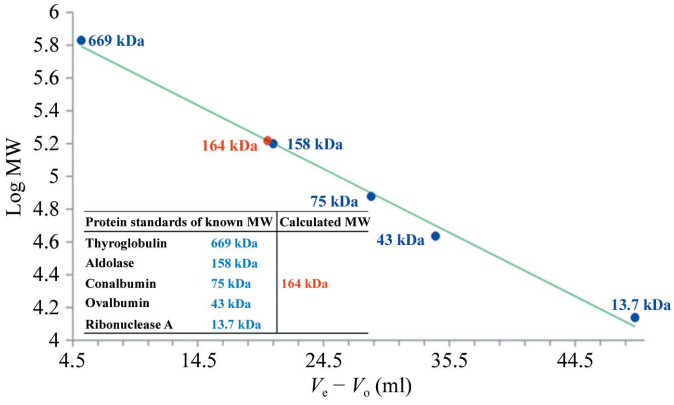

Figure 1
Tetrameric form of ERG10 in solution as analysed by analytical size-exclusion chromatography. The blue dots fitted with a green line correspond to protein standards of known molecular weights. The red dot indicates the target protein subjected to analysis.

3.3. Comparison of the binding pocket between ERG10 and T2

A high degree of sequence identity was found among ERG10, T2 and bCT. Sequence alignment of ERG10 with T2 and bCT helps us to determine the binding and catalytic residues in ERG10 (Fig. 3). Generally, the protein residues and their spatial orientations for binding the adenosine 3′-phosphate and pantetheine moieties of the CoA molecule are similar when ERG10 is superposed on T2 (Fig. 4*a*), suggesting that ERG10 has a similar CoA-binding mode. The β-mercaptoethylamine and pantothenic acid moieties of the CoA molecule were stabilized by Ser284 and His192 in T2. A crucial water molecule that hydrogen-bonds to His192 interacts with the pantetheine moiety *via* a hydrogen bond, as previously described by Haapalainen *et al.* (2007). In chain *B* of ERG10, Ser252 was found at the position corresponding to Ser284 in T2. A significant substitution of histidine by alanine (Ala159) was found in ERG10 at the position corresponding to His192 in T2 by sequence alignment. Consequently, the key water molecule is not observed at a similar position, which would further result in a loss of the hydrogen-bond interactions between the enzyme and substrate (Fig. 4*b*).

Apart from covering the active-site cavity, the covering loop also plays an important role in binding the pantetheine moiety of the CoA molecule by contributing another two residues to the binding pockets of T2 and bCT, which is in agreement with

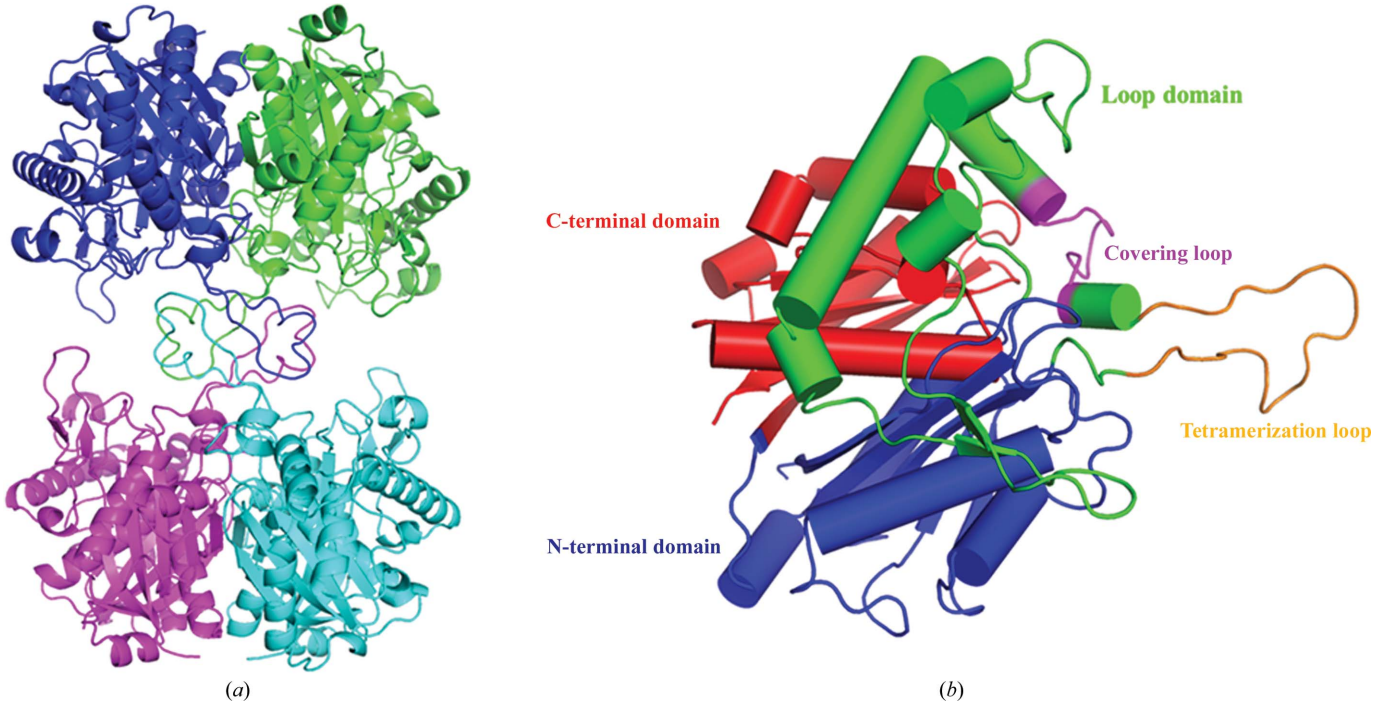

Figure 2
(*a*) Quaternary structure of the ERG10 tetramer generated by the dimerization of dimers. The tertiary structures of the four ERG10 monomers are distinguished by blue, green, magenta and cyan colours. (*b*) Overall cartoon representation of the ERG10 monomer. The N-terminal, C-terminal and loop domains are distinguished by dark blue, red and green colours, respectively. The covering loop is shown in purple and the tetramerization loop is shown in orange.

the residues (Leu151 and Met160) present at the same positions in the covering loop of ERG10. The surface-charge distributions of the covering loop are remarkably similar in T2 and bCT, but are significantly different in ERG10, with negative potential contributed by Ala159 and Glu156, respectively (Fig. 5).

Enzyme assays of T2 and bCT gave K_m values of 8 µ*M* (Haapalainen *et al.*, 2007) and 15 µ*M* (Masamune *et al.*, 1989) for acetoacetyl-CoA, respectively. The higher K_m value of 350 µ*M* for ERG10 as determined by Kornblatt & Rudney (1971) indicates a poor ability to bind the acetoacetyl-CoA molecule, probably owing to the substitution of histidine by alanine (Ala159) in the binding pocket, which is in line with the findings of Kim & Kim (2014), who reported that a His156Ala mutation in *Re*PhaA (a *β*-ketothiolase from *Ralstonia eutropha*) leads to a lower enzymatic activity

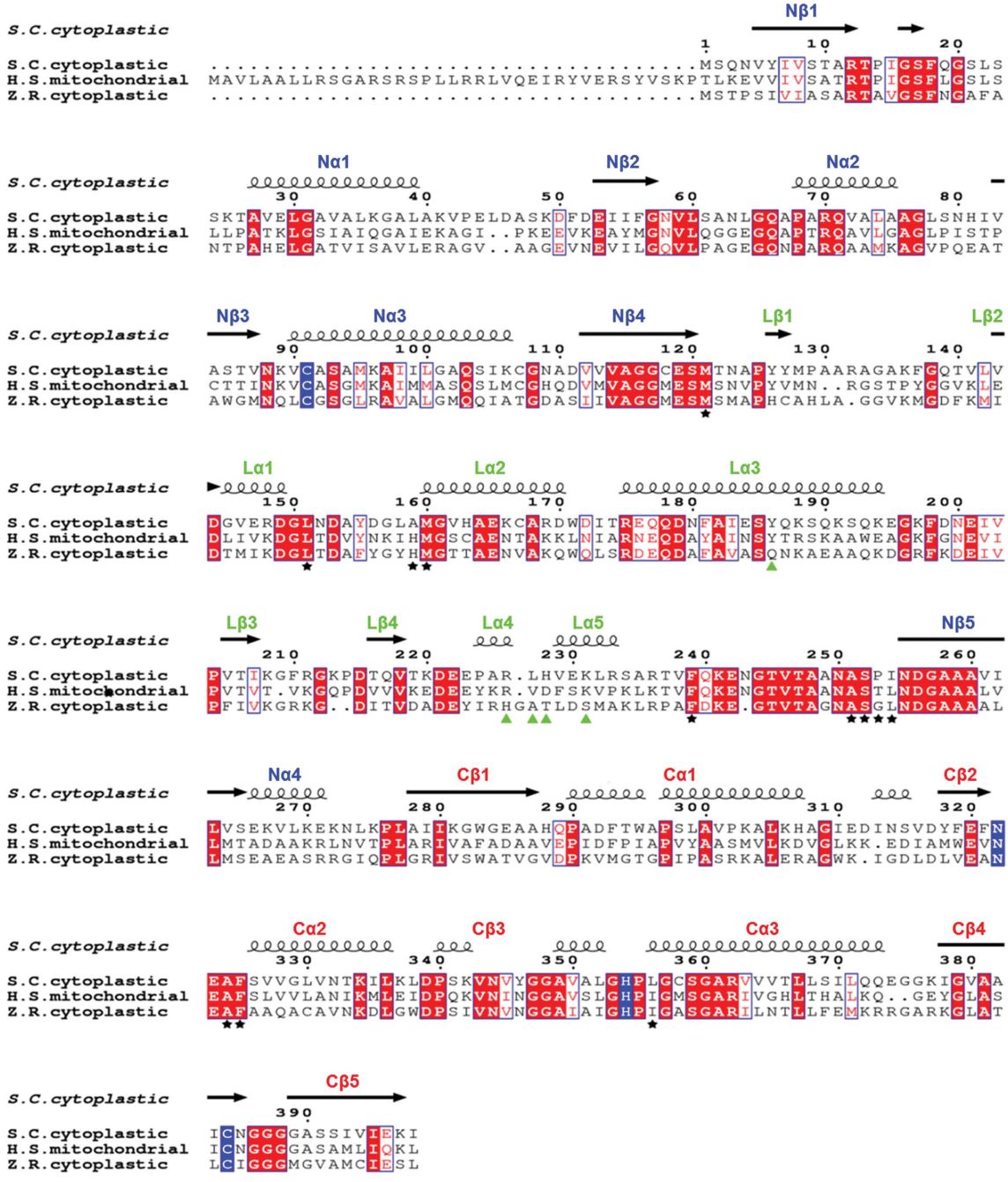

Figure 3
Sequence alignment of biosynthetic thiolases from various species (*S. cerevisiae*, *H. sapiens* and *Z. ramigera*). The secondary-structure elements of the *S. cerevisiae* cytosolic thiolase are shown based on the ERG10 structure. Residues that are conserved throughout the sequences are highlighted in red. Cys91, Asn322, His354 and Cys384 of the active site are represented in dark blue. The putative ERG10 residues for binding the adenosine 3′-phosphate and pantetheine moieties of the CoA molecule are marked with green triangles and black pentagons, respectively. The secondary-structure assignments were carried out and the figure was produced using *ESPript*3 (Robert & Gouet, 2014).

compared with the wild type. The impact of the negatively charged surface potential of the covering loop on the interaction between ERG10 and substrates remains unclear.

3.4. Implications of the disordered region and steric clashes

A high *B* factor indicates a lower possibility of finding an atom at its mean position in a crystal structure (Willis & Pryor, 1975). Residues in regions of high *B* factor are considered to be the result of dynamic disorder of the polypeptide chain or short-range or long-range disorder within the crystal (Deller *et al.*, 2016). During tracing and structure refinement of the ERG10 polypeptide chains, we found that residues Ala235–Asn250 of subunit *A* of ERG10 are missing in the electron density (Fig. 6) and have higher *B* factors than the corresponding regions of subunit *B* of ERG10 and the two subunits of the Cys91Ala mutant (Fig. 7). Hence, this polypeptide fragment is inherently disordered and was removed from the final structural model of ERG10. Missing regions of electron density in several proteins are likely to perform important

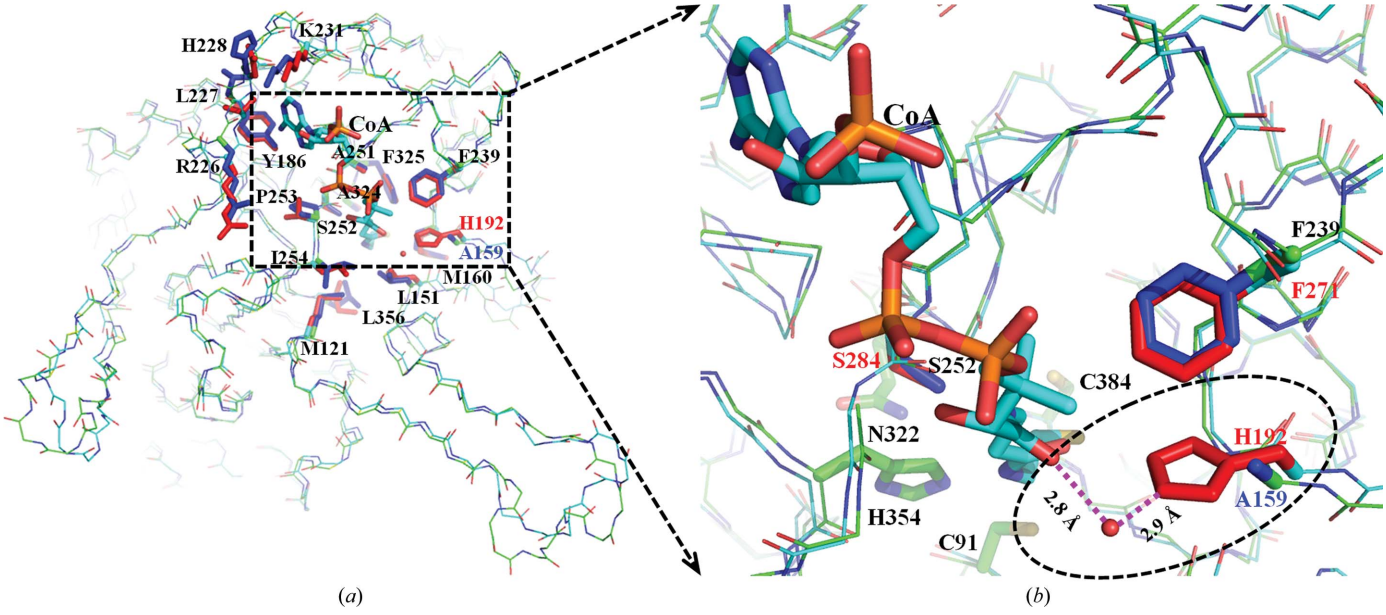

Figure 4
(*a*) A C^{α} trace showing a structural superposition of molecule *B* of ERG10 (green model) on T2 in complex with CoA (cyan model; PDB entry 2ibu). The side chains of residues involved in substrate binding are shown as blue (ERG10) or red (T2) sticks. (*b*) Close-up of the substrate-binding pocket to analyse the effect of the substitution of histidine by alanine (Ala159) causing the loss of certain hydrogen-bond interactions (indicated by purple dashed lines) between ERG10 and the pantetheine moiety of the CoA molecule. The Ala159 (ERG10) and His192 (T2) residues and the key water molecule at the entrance to the pantetheine-binding cavity are highlighted in the dotted ellipse as blue and red sticks and a red sphere, respectively. The architecture of the active site containing Cys91, Asn322, His354 and Cys384 (shown as green sticks) is also highlighted.

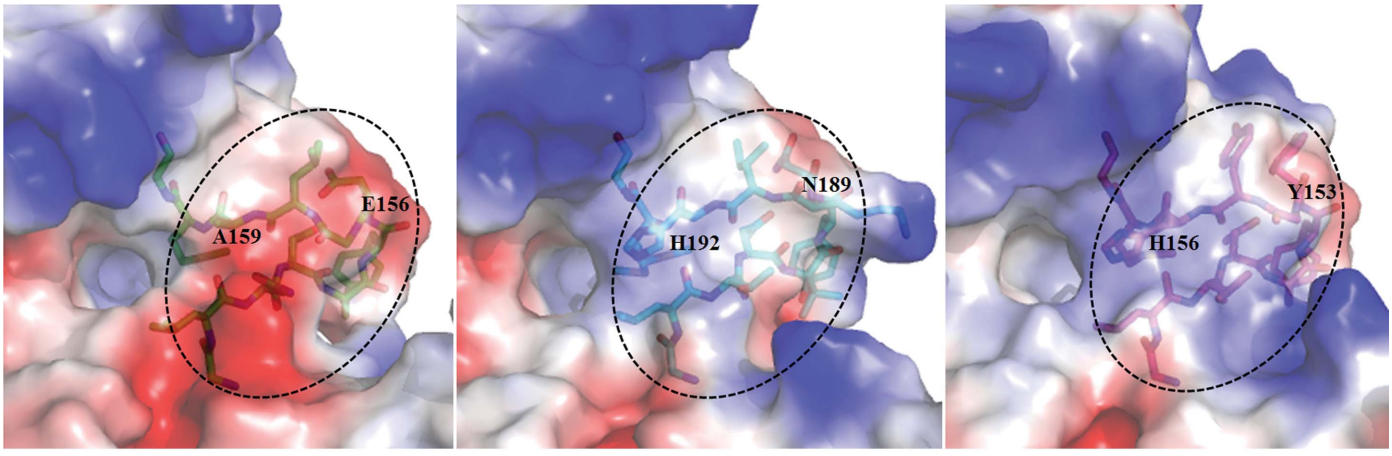

Figure 5
Surface-charge diagrams of (*a*) ERG10, (*b*) T2 and (*c*) bCT. Electrostatic surface potential diagrams were drawn in an identical orientation after superposition. The covering loops are shown as green, cyan and red stick models, respectively. His192 of T2, His156 of bCT and the corresponding Ala159 of ERG10 at the entrance to the pantetheine-binding tunnel are labelled. The negative potential of the covering loop, which is highlighted with a dotted ellipse, in ERG10 differs from the surface potential in T2 and bCT. The corresponding residues Glu156 (ERG10), Asn189 (T2) and Tyr153 (bCT) are also labelled.

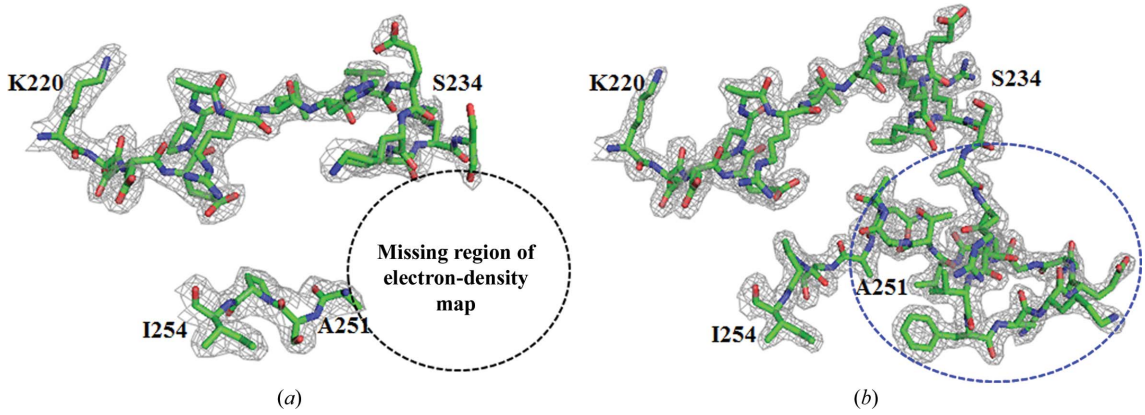

Figure 6
Comparison of the density maps of the peptide fragment Lys220–Ile254 from chain *A* of (*a*) the ERG10 and (*b*) the Cys91Ala mutant biosynthetic thiolases. The maps are weighted $2F_o - F_c$ maps contoured at 1.0σ and were calculated after refinement. The electron density in the blue ellipse is well defined in the Cys91Ala mutant but is missing in ERG10.

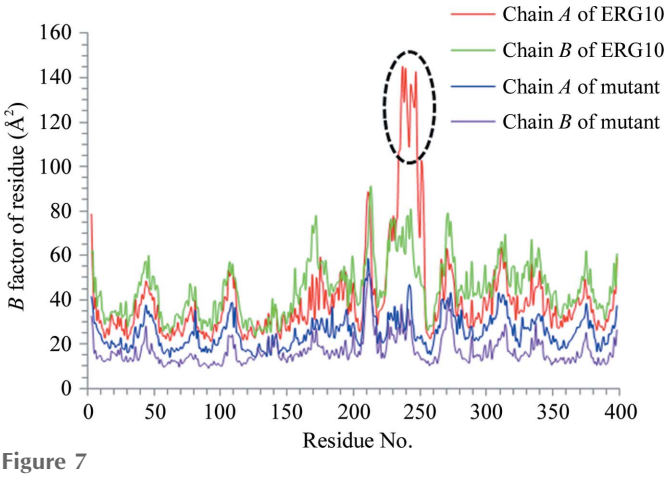

Figure 7
B-factor plots of the residues of four chains from ERG10 and its mutant. The *B*-factor distributions of the two chains of the Cys91Ala mutant are similar. Generally, the *B*-factor distributions of the two chains of ERG10 are also similar, disregarding residues Ala235–Asn250, which have the highest *B* factors, as indicated by the black ellipse.

functions, as reported by Huber & Bennett (1983). This peptide fragment may provide Phe239 to bind the pantetheine moiety of the CoA molecule by hydrophobic interactions (Fig. 4*b*).

As shown in Fig. 8(*a*), structural superposition of the two subunits in the asymmetric unit of ERG10 shows an ordered conformation in the corresponding region in subunit *B*, whereas a flexible conformation and obvious polypeptide-chain movements are observed at both ends of the disordered region in subunit *A*. Furthermore, superposition of subunit *A* of apo ERG10 and the structure of T2 in complex with a CoA molecule revealed significant structural differences between the binding pocket at the C^{α} atoms of His228 (2.0 Å from the C^{α} atom of Asp260 in T2) and Ser252 (5.5 Å from the C^{α} atom of Ser284 in T2). The differences in the positions of these two residues would lead to steric clashes with the adenine and pantetheine moieties of the CoA molecule, respectively (Fig. 8*b*), which raises the possible hypothesis that binding of the CoA molecule induces conformational changes, as has

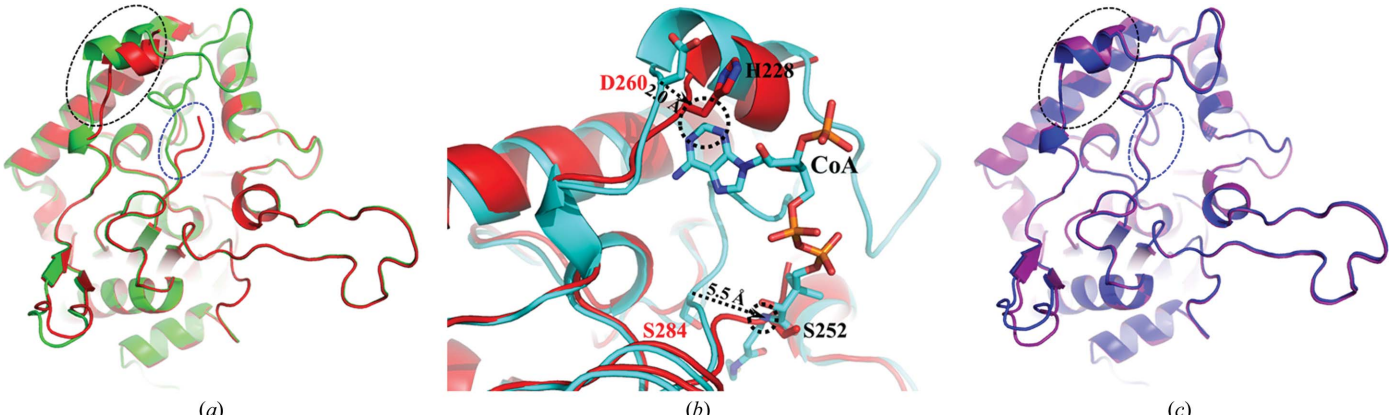

Figure 8
Comparison of structural superpositions of molecule *A* (red or blue cartoon model) onto molecule *B* (green or purple cartoon model) of (*a*) ERG10 and (*c*) the Cys91Ala mutant. Polypeptide-chain movements occur at the N-terminus and C-terminus of the disordered region only in molecule *A* of ERG10, as indicated by the black and blue ellipses, respectively. The two corresponding regions in the Cys91Ala mutant with identical conformation are also indicated by black and blue ellipses, respectively. (*b*) A CoA molecule was docked into molecule *A* of ERG10 (red cartoon model) by superposing it on molecule *A* of T2 (cyan cartoon model; PDB entry 2ibu) in complex with a CoA molecule. His228 and Ser252 of molecule *A* of ERG10, which clash significantly with the docked CoA molecule, are highlighted with black circles.

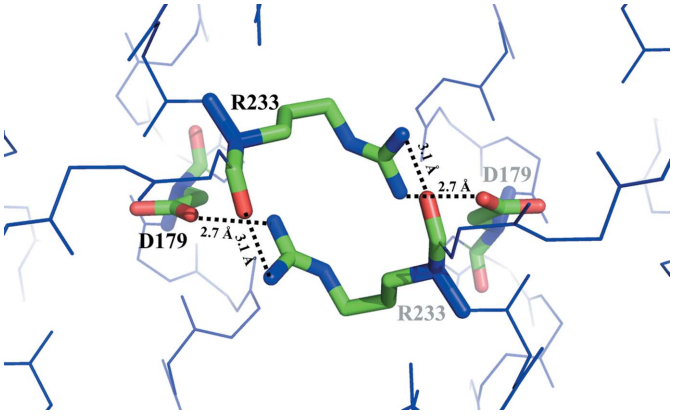

Figure 9
The close contact of the peptide fragment between molecules *A* (shown as blue C^{α} traces) of two neighbouring asymmetric units in the Cys91Ala mutant is formed by hydrogen bonds (indicated as black dashed lines) between Arg233 and Arg233 and between Arg233 and Asp179 (shown as green sticks).

been commonly observed but which remains unreported in the thiolase superfamily.

Protein folding is affected by many factors, including pH, primary structure, ligand binding and crystal packing (Deller *et al.*, 2016). The peptide fragment Ala235–Asn250 is involved in crystal packing in both the native protein and the Cys91Ala mutant (Fig. 9). The stable conformation of the peptide fragment (Fig. 8*c*) prompts us to speculate that the slightly tighter crystal packing in the mutant is perhaps a result of the CoA molecule binding but with differential occupancy. Further research is required to explore the impact of Ala159 on the affinity, and the structure of the ligand-bound mutant would be useful to test our hypothesis on the conformational changes involved in ligand binding.

Acknowledgements

We thank the staff at beamline BL17U1 of the Shanghai Synchrotron Radiation Facility (SSRF) and beamline BL18U1 of the National Facility for Protein Science (NFPS) at SSRF for assistance during data collection.

Funding information

This work was supported by the Chinese National Natural Science Foundation (grant Nos. U1632124, 31270770 and 31621002) and the Chinese Ministry of Science and Technology (grant Nos. 2017YFA0503600 and 2017YFA0504903).

References

DeLano, W. L. (2002). *CCP4 Newsl. Protein Crystallogr.* **40**, 82–92. http://www.ccp4.ac.uk/newsletters/newsletter40/11_pymol.html.
Deller, M. C., Kong, L. & Rupp, B. (2016). *Acta Cryst.* F**72**, 72–95.
Emsley, P., Lohkamp, B., Scott, W. G. & Cowtan, K. (2010). *Acta Cryst.* D**66**, 486–501.
Haapalainen, A. M., Meriläinen, G., Pirilä, P. L., Kondo, N., Fukao, T. & Wierenga, R. K. (2007). *Biochemistry*, **46**, 4305–4321.
Haapalainen, A. M., Meriläinen, G. & Wierenga, R. K. (2006). *Trends Biochem. Sci.* **31**, 64–71.
Hiser, L., Basson, M. E. & Rine, J. (1994). *J. Biol. Chem.* **269**, 31383–31389.
Huber, R. & Bennett, W. S. (1983). *Biopolymers*, **22**, 261–279.
Jiang, C., Kim, S. Y. & Suh, D.-Y. (2008). *Mol. Phylogenet. Evol.* **49**, 691–701.
Kim, E.-J. & Kim, K.-J. (2014). *Biochem. Biophys. Res. Commun.* **452**, 124–129.
Kornblatt, J. A. & Rudney, H. (1971). *J. Biol. Chem.* **246**, 4417–4423.
Kursula, P., Sikkilä, H., Fukao, T., Kondo, N. & Wierenga, R. K. (2005). *J. Mol. Biol.* **347**, 189–201.
Laskowski, R. A., MacArthur, M. W., Moss, D. S. & Thornton, J. M. (1993). *J. Appl. Cryst.* **26**, 283–291.
Masamune, S., Walsh, C., Sinskey, A. & Peoples, O. (1989). *Pure Appl. Chem.* **61**, 303–312.
Mathieu, M., Modis, Y., Zeelen, J. P., Engel, C. K., Abagyan, R. A., Ahlberg, A., Rasmussen, B., Lamzin, V. S., Kunau, W. H. & Wierenga, R. K. (1997). *J. Mol. Biol.* **273**, 714–728.
Modis, Y. & Wierenga, R. K. (1999). *Structure*, **7**, 1279–1290.
Modis, Y. & Wierenga, R. K. (2000). *J. Mol. Biol.* **297**, 1171–1182.
Murshudov, G. N., Skubák, P., Lebedev, A. A., Pannu, N. S., Steiner, R. A., Nicholls, R. A., Winn, M. D., Long, F. & Vagin, A. A. (2011). *Acta Cryst.* D**67**, 355–367.
Otwinowski, Z. & Minor, W. (1997). *Methods Enzymol.* **276**, 307–326.
Robert, X. & Gouet, P. (2014). *Nucleic Acids Res.* **42**, W320–W324.
Sato, T., Kanai, Y. & Hoshino, T. (1998). *Biosci. Biotechnol. Biochem.* **62**, 407–411.
Vagin, A. & Teplyakov, A. (2010). *Acta Cryst.* D**66**, 22–25.
Willis, B. T. M. & Pryor, A. W. (1975). *Thermal Vibrations in Crystallography*. Cambridge University Press.